THE INFLUENCE OF PRINT LAYER ORIENTATION ON THE MECHANICAL PROPERTIES OF SIC AND C_F/SIC CMCS FORMED VIA DIRECT INK WRITING

by

Kyle Cox

A Thesis

Submitted to the Faculty of Purdue University

In Partial Fulfillment of the Requirements for the degree of

Master of Science in Materials Engineering

School of Materials Engineering

West Lafayette, Indiana

December 2021

THE PURDUE UNIVERSITY GRADUATE SCHOOL
STATEMENT OF COMMITTEE APPROVAL

Dr. Rodney Trice, Co-Chair

School of Materials Engineering

Dr. Jeffery Youngblood, Co-Chair

School of Materials Engineering

Dr. Carlos Martinez

School of Materials Engineering

Approved by:

Dr. David Bahr

Dedicated to my family. Without their support,
none of this would have been possible, and I would not be where I am today.

ACKNOWLEDGMENTS

I would like to thank the Purdue Military Research Institute (PMRI) and its leaders, Prof. Eric Dietz and Mr. Dave Hankins, for their financial and professional support while I was attending Purdue University. I would like to thank Spectral Energies for their financial support of the work found in the appendix. I would also like to thank my advisors, Prof. Rodney Trice and Prof. Jeffery Youngblood, for all of their support and guidance. Additional thanks to Prof. Carlos Martinez for being the third member of my committee. I would also like to thank members of the Trice and Youngblood research groups, namely Rodrigo Orta-Guerra, Olivia Brandt, Averyonna Kimery, Abdulla Al Saad, and Ashwin Sivakumar. Special thanks is also directed to my lab partner Tess Marconie and our undergraduate researcher Karan Motwani. Without their help, this work would not be where it is today.

Chapter 1 of this thesis is in the process of being submitted for publication to the journal *Additive Manufacturing*. Authors are listed as: Kyle Cox, Tess Marconie, Karan Motwani, Jeffery Youngblood, and Rodney Trice.

The views expressed in this thesis are those of the author and do not reflect the official policy or position of the United States Air Force, Department of Defense, or the U.S. Government.

TABLE OF CONTENTS

LIST OF TABLES

LIST OF FIGURES

ABSTRACT

Silicon carbide is a useful monolithic and matrix ceramic due to its excellent mechanical properties and corrosion/oxidation resistance at high temperature. This makes it an attractive material for use in advanced applications, such as aircraft engines and high-speed flight. In this study, additively manufactured monolithic SiC and C_f/SiC CMCs, processed via direct ink writing (DIW) of a 53 vol% colloidal suspension, achieved >96% theoretical density through pressureless sintering. When present, fibers are aligned in the direction of the print path. Five different print paths were studied, including a 0^o path, 90^o path, $0/90^o$ path, $0/15/30/45/60/75/90^o$ path, and $0/30/60/90/60/30/0^o$ path. Four-point bend testing was performed to determine flexural strength and Weibull analysis was performed. Strengths were highest for the 0^o print path. The characteristic strength, σ_o, of this print path was 375 MPa with a Weibull modulus of 7.4 for monolithic SiC and a σ_o of 361 MPa with a Weibull modulus of 10.7 for C_f/SiC. Weibull modulus was greater for C_f/SiC samples compared to identically printed monolithic SiC samples. SEM and optical microscopy were used to analyze printed parts which showed a high degree of fiber alignment in the direction of the print. Fiber pullout was observed on the fracture surface, as well as intragranular fracture.

1. THE INFLUENCE OF PRINT LAYER ORIENTATION ON THE MECHANICAL PROPERTIES OF SIC AND C_F/SIC CMCS FORMED VIA DIRECT INK WRITING

1.1 Introduction

Silicon Carbide is a useful ceramic for its excellent mechanical properties. It has extremely high strength and oxidation and corrosion resistance for temperatures up to 1500 ^oC.[1,2,3] SiC is an extremely useful ceramic for many advanced applications such as reactor coatings, heat exchangers, and harsh environments such as in high-speed flight, aircraft engines or leading edges.[2,3,4] In order to be used in these types of applications, a high density is required. High densities lead to better mechanical properties, as failure often occurs at defects such as pores. A common technique for densification of SiC is hot pressing. This sintering technique applies high pressure and high heat to densify the ceramic. Wang et al.[5] were able to achieve strengths of 647 MPa and a fracture toughness of 5.0 MPa $m^{1/2}$ by hot-pressing SiC. However, the main drawback of hot-pressing is the inability to process complex shapes. Pressureless sintering allows for geometries to be created that would not normally be sinterable via hot-pressing.

Most ceramics are formed from ceramic powders, and sintered to achieve a solid, dense part. Colloidal powders are often combined with a solvent to create suspensions, which offer many advantages for ceramic processing. Since the powder is suspended in a liquid, it can be used for casting or slip casting, a very common technique.[6,7] A more advanced technique, injection molding, has been accomplished with colloidal suspensions of alumina,[8] silicon nitride,[9,10] boron carbide,[11] and zirconium diboride.[12] In injection molding, the aqueous suspension in extruded under pressure into a mold. The external pressure forces the suspension to fill all parts of the mold. The mold is removed, and then the part is sintered.

Additive manufacturing (AM) allows for the creation of complex geometries that are not attainable using other processing techniques. While AM for ceramics is more limited in scope when compared to polymers or metals, there are still 2 main avenues of manufacture. Binder jetting involves selectively dropping liquid binder into a ceramic powder bed, and building up the part layer by layer. The part is then removed from the powder bed and sintered. This was demonstrated using a geopolymer containing a mixture of ceramic powders.[13] Additionally, Zocca et al.[14] made

Si/SiC by creating a SiC part in a powder bed, and then infiltrating liquid silicon to densify the part. An alternative method to AM of ceramics is DIW. Like many common ceramic forming techniques, it commonly utilizes a colloidal suspension. Additionally, DIW does not require the large powder beds used in binder jetting, which are expensive and required additional safety measures.

For DIW, the colloidal suspension is extruded through a nozzle and is laid down layer by layer until a part is built up, similar to polymer extrusion 3D printers. DIW can be accomplished using a variety of colloidal suspensions, including various carbides, [2,15,16,17] oxides,[16,18] nitrides,[10] and borides.[19] The solvent is removed by drying, leaving a ceramic green body. The green body contains the ceramic powder and polymer binders. The binders are then burned out in a furnace to create a brown body, which is then sintered to create a dense part. Pressureless sintering is most common, as it provides the ability to maintain the desired geometry. DIW can also be accomplished by using cements,[20,21,22] or even a preceramic polymer.[1,19,23,24,25] However, using a preceramic polymer can create large amounts of unwanted porosity, which is a major drawback to this type of DIW.[4] DIW has many advantages when compared to other non-AM ceramic processing techniques. It provides the ability to print geometrically complex parts.[1,2,15] While this is possible with other techniques such as slip casting or injection molding, DIW does not require molds or additional tooling. It also allows for easy modification of designs and rapid prototyping of parts. Additionally, DIW has the ability to align fibers to create CMCs.

Aligning fibers can enhance the mechanical properties of a ceramic and create a ceramic matrix composite (CMC). In a CMC, a high aspect ratio particle can be used as a reinforcement phase. The ceramic is normally reinforced by fibers, platelets, or whiskers.[1,19,23,25,26] When fibers are added to the matrix, they provide crack bridging and fiber pullout.[1,23,24] These effects provide crack deflection and lengthen the crack, with the ultimate goal of improving mechanical properties. DIW has the ability to align fibers in the direction of the print. The alignment is caused by the shear stresses experienced as the fibers pass through the nozzle.[23] Fibers are most commonly incorporated into a suspension that contain a preceramic polymer.[1,19,24] However, this process involves extra processing steps, such as pyrolysis or infiltration, which results in lower porosity.[4] In order to achieve fiber alignment and a high density, fibers can be added directly to a colloidal suspension. This removed the need for pyrolysis or infiltration steps, and offers the ability to sinter

to high densities. Kemp et al.[19] added SiC fiber directly to a colloidal suspension of zirconium diboride, although they still used a preceramic polymer as a binder and to help create a SiC phase.

This research aims to create carbon fiber reinforced silicon carbide (C_f/SiC) CMCs via DIW. Milled carbon fiber is added directly to a highly loaded colloidal suspension of SiC, without the use of any preceramic polymer, which is then sintered to a high density via pressureless sintering. The fiber alignment is controlled by the direction of the print layers, since the fibers should be aligned in the direction of the print path. The print path is then changed from print to print to determine the effect print direction and fiber alignment has on the mechanical properties of the C_f/SiC CMC. Flexure strength was used to determine the change in mechanical properties. Weibull analysis was utilized to determine the distribution of defects within the prints and their effects on strength.

1.2 Methods

1.2.1 Powder Preparation

The powder used for printing was prepared by mixing 600 nm β-SiC powder (US Research Nanomaterials, Houston, TX.), 400 nm alumina (Almatis, A16, Frankfort, Germany), and 0.5-1 µm yttria (SkySpring Nanomaterials Inc., Houston, TX). The powder mixture contained 4 wt% yttria, 6 wt% alumina, and 90 wt% SiC. The yttria and alumina act as sintering aids and form a liquid phase during sintering to help promote densification. The powders were mixed in 200 proof ethanol and ball milled for 24 hours with 1 cm WC milling media at 50 rpm. After milling, the ethanol was removed by rotary evaporation followed by drying at 115 ^{o}C for 12 hours.

1.2.2 Suspension Preparation

Polyethyleneimine (PEI, Mn 10,000, Branched, Sigma-Aldrich Inc., Germany) was selected as the dispersant, polyvinylpyrrolidone (PVP, Mn 55,000, Sigma-Aldrich, US) was used as a viscosity modifying agent, and HCl (38%, Fisher Chemical, Canada) was used to adjust the pH. Suspensions were made to contain 53 vol% solids (SiC, sintering aids, carbon fiber), 2.16 vol% PEI, 0.20 vol% PVP, 0.93 vol% HCl, and balanced water. Liquids and polymers were mixed first, followed by addition of 2, 1 cm WC milling media and solids. All suspensions were mixed in a FlackTek DAC 1200-300 Speedmixer (Landrum, SC), with the container scraped with a spatula between each round of mixing. A round consists of 3 minutes, with one minute each of 800 rpm, 1200 rpm, and 1600 rpm. After mixing, the suspensions were rolled on a ball mill at 50 rpm for 21-23 hours. After milling, the suspension was mixed one additional time in the Speedmixer for 3 minutes before being degassed. Degassing occurred under vacuum with 200 rpm mixing for 5 minutes. The suspension was then loaded into a 60 mL syringe with vibration. Suspensions without carbon fiber are denoted as monolithic SiC suspensions.

Milled carbon fiber (80 µm length, 7 µm diameter, Composite Envisions, Wausau, WI) was added to the suspension in the amount of 10 vol% of the solids loading, which would ultimately become 10 vol% of the sintered part. The fibers were received without any sort of coating or interface layer. No additional surface treatment was applied to the fibers before or during mixing. The fiber was added after the mixing of the water, polymer, and HCl, but before the

addition of the WC milling media and powder. The amount of PVP was increased to 0.30 vol% to increase the viscosity and improve printability. No modifications were made to the powder, the mixing process, or the syringe loading process. Suspensions with carbon fiber are denotated as C_f/SiC suspensions.

1.2.3 Rheology

Rheology measurements were taken on a Malvern Instruments Bohlin Gemini 200 HR Nano Rheometer (Worcestershire, UK). Parallel plate geometry was used with a gap size of 1 mm. The temperature was set to 25 ^oC and a solvent trap and ultrasonic humidifier were used to prevent the suspension from drying during the test. Before the test, a pre-shear of 50 s^{-1} was applied for 1 minute followed by 1 minute of rest.

1.2.4 Printing

All billets were printed on a Hyrel 3D System 30M 3D printer (Norcross, GA) using an SDS-60 print head and 60 mL Luer Lock syringes. Nozzles were 5 cm long, and had an internal diameter of 1.4mm at the opening. This nozzle size was selected because the suspension experiences higher shear stresses with a narrow nozzle, which leads to greater alignment.[23] However, nozzle clogging is affected by nozzle size and geometry.[27] This exact nozzle was selected to prevent clogging while still being narrow enough to allow sufficient fiber alignment. An ultrasonic humidifier was used on the lowest setting to add humidity to the atmosphere inside of the printer. This prevented suspension from drying during printing. A nozzle velocity of 4 mm/s was used. Slic3r software was used to slice the prints and to create G-code. The G-code was then modified in house to achieve the desired print layer orientations.

Figure 1.1. shows an example of each print path. The billets printed were 60x40x7 mm, and were 7 layers tall. Each layer was 1 mm in thickness. Bend bars were cut so the length was in the 60 mm direction. The angles for the print layers were designated as 0^o in the direction of the 60 mm side, and 90 ^{o} along the 40 mm side. A total of 5 print layer orientations were printed. 0^o prints had all print paths running in the 0^o direction. This results in all print lines running along the length of the bend bars. 90^o prints had all print paths running in the 90^o direction, which would be perpendicular to the length of the bend bar. $0/90^o$ "crosshatched" prints had the print path alternate

each layer between going in the 0^o and 90^o directions, starting and finishing in the 0^o direction. A $0/15/30/45/60/75{90}^o$ print had print paths that rotated 15^o each layer, starting in the 0^o direction and finishing in the 90^o direction. This was an asymmetric print, and the side with the 0^o direction was tracked and placed in tension in the bend test. Moving forward, this print orientation will be designated as "15^o". A $0/30/60/90/60/30/0^o$ print was also printed. In this symmetric print, the print path direction changed by 30^o each layer, starting and ending with the 0^o direction. This print will be referred to as "30^o." All print paths were printed with both SiC and 10 vol% C_f/SiC suspensions.

Upon the completion of printing, the printed billets were immediately placed into a humidity oven to dry for 48 hours at 95% relative humidity and 35 ^{o}C. All billets remained in the humidity oven after drying until binder burnout. Drying in this method prevented cracking of the green bodies.

1.2.5 Binder Burnout and Sintering

Binder burnout was completed in a Carbolite Gero tube furnace (Neuhausen, Germany). Samples were heated at a rate of 0.5 ^{o}C/min to 600 ^{o}C, followed by a 3-hour hold. Ar was used a carrier gas. A Carbolite Gero LHTG 200-300/301G resistively heated graphite furnace (Neuhausen, Germany) was used for pressureless sintering. Billets were heated at a rate of 25 ^{o}C/min to 1950 ^{o}C, followed by a 2-hour hold, and then cooled to room temperature. An Ar atmosphere was maintained throughout sintering. All billets were sintered in a powder bed with the same composition as the starting powder. Density was calculated using Archimedes' method. The theoretical density of SiC with sintering aids is 3.294 g/cm^3, and with the addition of 10 vol% carbon fiber, the theoretical density drops to 3.145 g/cm^3; both calculated using the rule of mixtures.

1.2.6 Machining

Only fully sintered billets were machined into bend bars to be tested. MIL-STD 1942 B specimen bend bars were machined in accordance with ASTM C1161-18[28] on a Kent USA SGS-1020 AHD surface grinder (Tustin, CA). Bend bar dimensions, b and d, were 4 and 3 mm respectively. Special care was taken to cut the bend bars to avoid including any visible cracks that occurred during sintering. The ends of bars were not machined.

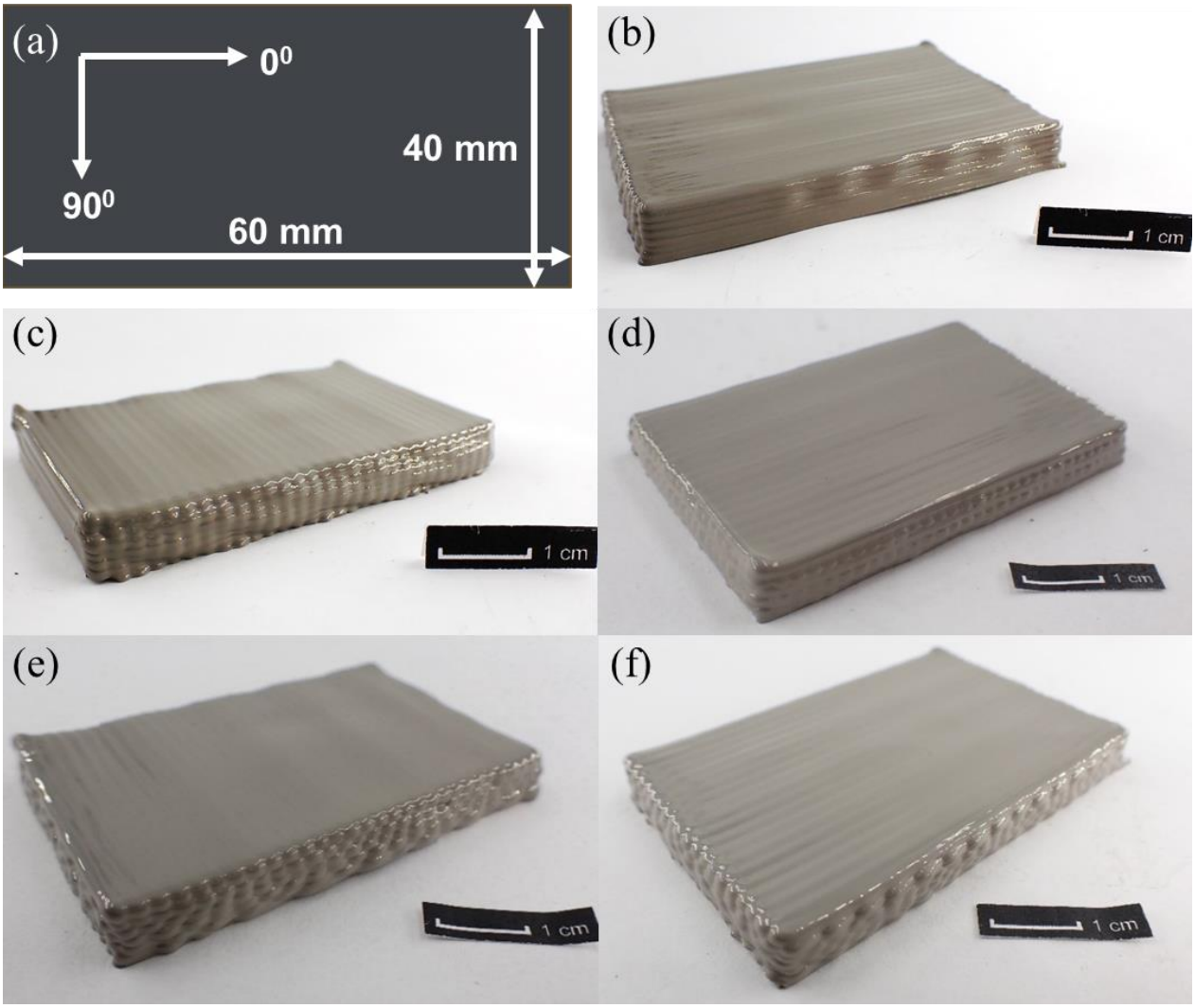

Figure 1.1. One example of each print orientation is shown. There was no observable difference between monolithic SiC and C_f/SiC billets. (a) Reference axis and dimensions for print orientation. The gray rectangle represents a printed billet. (b) A monolithic SiC 0º Print. (c) A monolithic SiC 90º Print. (d) A monolithic SiC 0/90º Print. (e) A monolithic SiC "15º" Rotation Print. (f) A monolithic SiC "30º" Rotation Print.

1.2.7 Flexure Testing

Flexure testing was accomplished on a 100 kN MTS Insight load frame. (Eden Prairie, MN). A semi-articulating 4-point test fixture was used. Contact points were steel cylinders. The test was conducted in accordance with ASTM C1161-18 standards.[28] Testing was conducted on 3 separate days with humidity of 23%, 46%, and 56% humidity. All tests were conducted at room temperature. The test was displacement controlled with a constant crosshead displacement of 0.5 mm/s. All bend bars were inspected and any visible flaws were placed on the compression side of the test. The exception to this is "15º" bend bars, which were placed with the side that originally had the 0º direction in tension. Strengths were calculated from the peak load before failure, and each sample contained between 13-15 bend bars.

1.2.8 Fiber Alignment

A 10 vol% C_f/SiC suspension was cast into a mold under vibration to create a pellet. This pellet serves as a baseline for a random distribution of fiber angles, since there was no induced fiber alignment with this method. This is then compared to the fiber alignment achieved in a C_f/SiC 0º printed sample. Samples for fiber alignment were cut to expose a cross section from the middle of the sample and then mounted in epoxy for polishing. The surface of the cast pellet analyzed is parallel to the bottom of the pellet, and the printed sample was cut in the direction parallel to the print path.

Polishing occurred on a LECO GPX200 auto polisher (St. Joseph, MI). Every sample was polished to 1 µm until all visible surface scratches were removed. Images were taken in an AmScope optical microscope fitted with an 18 MP Aptina Color CMOS digital camera (AmScope) using 5x, 10x, and 50x magnification. Angles were measured using ImageJ, an open-source image analyzing software. Angles were measured from multiple areas on the sample. For the cast pellet, the angles were measured relative to a nominal 0º direction, which was designated as parallel to the bottom edge of the image. Angles for printed samples were measured relative to the bottom edge of the bend bar. A total of 46 fibers were measured for the cast pellet and 34 fibers for the printed sample.

An order parameter (S) was calculated for each measured fiber angle.[29,30] Order parameter ranges from [0:1], with S=1 being perfect alignment. The average order parameter was calculated.

This alignment is only measured on a two directional plane. It does not factor in alignment of fibers into or out of the plane. These calculations and images only serve to show that this DIW process can create aligned fibers within a SiC matrix. This serves as a way to quantify that alignment and compare it to a more traditional processing technique.

Fracture surfaces were analyzed in a Quanta 3D, FEG SEM (Hillsboro, OR), looking at the fracture surface. Fiber pullout was measured on the same SEM, but looking at the side of the fracture surface. Pulled out fiber lengths were measured in ImageJ.

1.3 Discussion

1.3.1 Rheology

Figure 1.2. shows the loss and storage modulus plots and viscosity curves for the SiC and C_f/SiC suspensions used. Both the monolithic SiC and the C_f/SiC suspensions exhibited yield-pseudoplastic rheology. The viscosity vs. shear rate curves show that both suspensions were shear thinning, however, the C_f/SiC suspension is less thixotropic. A similar shear thinning behavior is seen in other colloidal suspensions in literature. DIW with colloidal SiC,[2,17] as well as B_4C[15] and Al_2O_3,[17,18] used a shear thinning suspension.

The yield stress was calculated at the point where the storage modulus (G') crosses the loss modulus (G'').[17] The yield stress for the monolithic SiC suspension was 120 Pa and for the C_f/SiC suspension was 30 Pa. The yield stress was lower for the C_f/SiC suspension, however there was no slumping observed during printing. Additionally, for this study, printability was the only factor of interest. Both suspensions were extrudable and printable with acceptable print quality. No further tailoring of the rheology was tested. The full extent of the effect of the carbon fibers on suspension rheology is an area for future study.

1.3.2 Density

The average density for monolithic SiC bend bars was 96.4 ±0.48% theoretical density (TD) a range from 94.9-97.5% TD. The average density for C_f/SiC bend bars was 96.2 ±0.45% TD and a range from 94.1-98.1% TD. No pattern was observed between specific print orientation and density. Figure 1.3. shows the densities of sintered parts with various amounts of carbon fiber. Pellets were cast under vibration containing the specified amount of carbon fiber. All printed samples were printed according to the stated procedures. Binder burnout and sintering were identical for all samples and followed the procedures above. Density drops with amount of fiber loading after 5 vol% fibers are added. There are more fiber-fiber interactions with increasing fiber loading, which results in higher porosity and lower densities. The densities of 0 vol% fiber prints are lower than cast pellets because porosity is introduced at the interfaces between layers and as air bubbles entrapped in the print roads. Printed samples with carbon fibers do not drop in density at the same

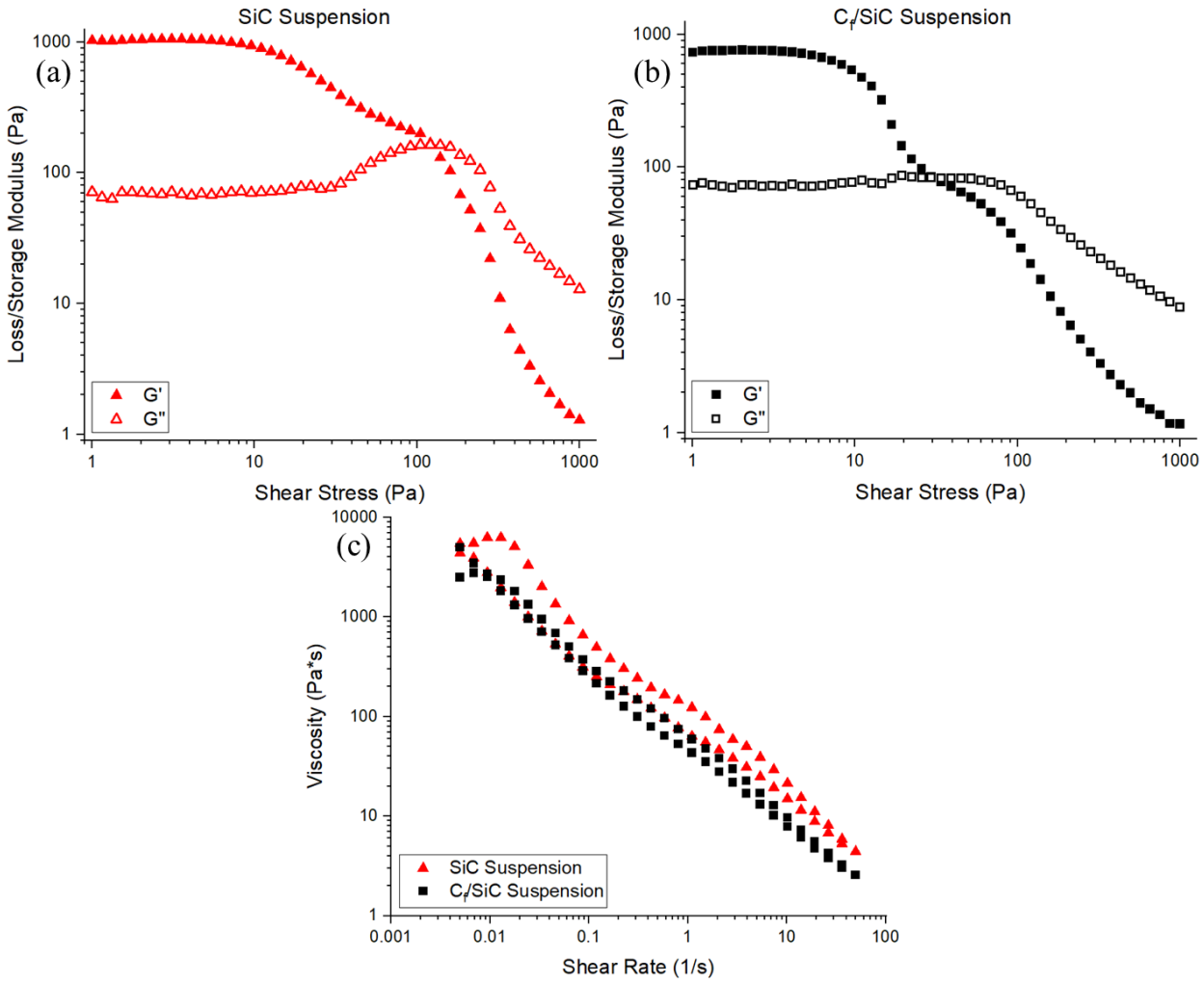

Figure 1.2. (a) The loss and storage modulus vs. shear stress for the SiC suspension. (b) The loss and storage modulus vs. shear stress for the C_f/SiC suspension. (c) The viscosity curves of both the SiC and C_f/SiC suspensions showing shear thinning behavior.

rate as cast pellets because the fibers are aligned during printing. This reduces the amount of fiber/fiber interactions and the amount of associated porosity. 10 vol% carbon fiber was chosen as the amount of fiber to add because the printed samples had densities that were still above 95 %TD. Maintaining a high density is important. Xiong et al.[25] showed that as density increased, strength also increased. Therefore, in order to maintain a high strength, a high density is required.

1.3.3 Part Quality

Prints with carbon fiber tended towards cracking or warping upon sintering. "15º" prints and "30º" prints with carbon fiber displayed warping as shown in Figure 1.4. During sintering, the SiC matrix shrinks, but the carbon fibers do not shrink. The shrinkage was measured in both monolithic prints and fiber reinforced prints. For monolithic prints, the shrinkage was uniform across all print orientations at 14.8% shrinkage in both length and width of the billet, with the thickness shrinking by 13.2%. The shrinkage in C_f/SiC prints depended on the print direction. In prints with unidirectional fiber alignment, the shrinkage in the direction of the fiber was only 6.2% and the shrinkage in the opposite direction was 18.3%. In the 0/90º orientation prints, the shrinkage was 11.2% in both directions, since the fibers were aligned in both directions. This asymmetric shrinking caused minor cracking in the SiC matrix, roughly parallel to the direction of the fiber alignment.

The warping and cracking observed in Figure 1.4. is due to the asymmetric nature of the print and the carbon fibers not shrinking. Due to the warping of the C_f/SiC "15º" and "30º" prints, these samples were not able to be tested. Additionally, the "30º" prints of monolithic SiC were not tested. Any prints that cracked, but did not exhibit warping, were machined to remove the crack and were made into bend bars and tested.

1.3.4 Fiber Alignment

Figure 1.5. shows the results of fiber alignment measurements. Figure 1.5.(a) shows a more disordered distribution of fibers, especially when compared to the printed sample shown in Figure 1.5.(c). The fibers visually appear much more aligned in the printed sample. Additionally, the distribution is much narrower for the printed sample. These results are also shown with the order parameter. For the cast pellet S=0.34, and for the printed sample S=0.98. This shows that the

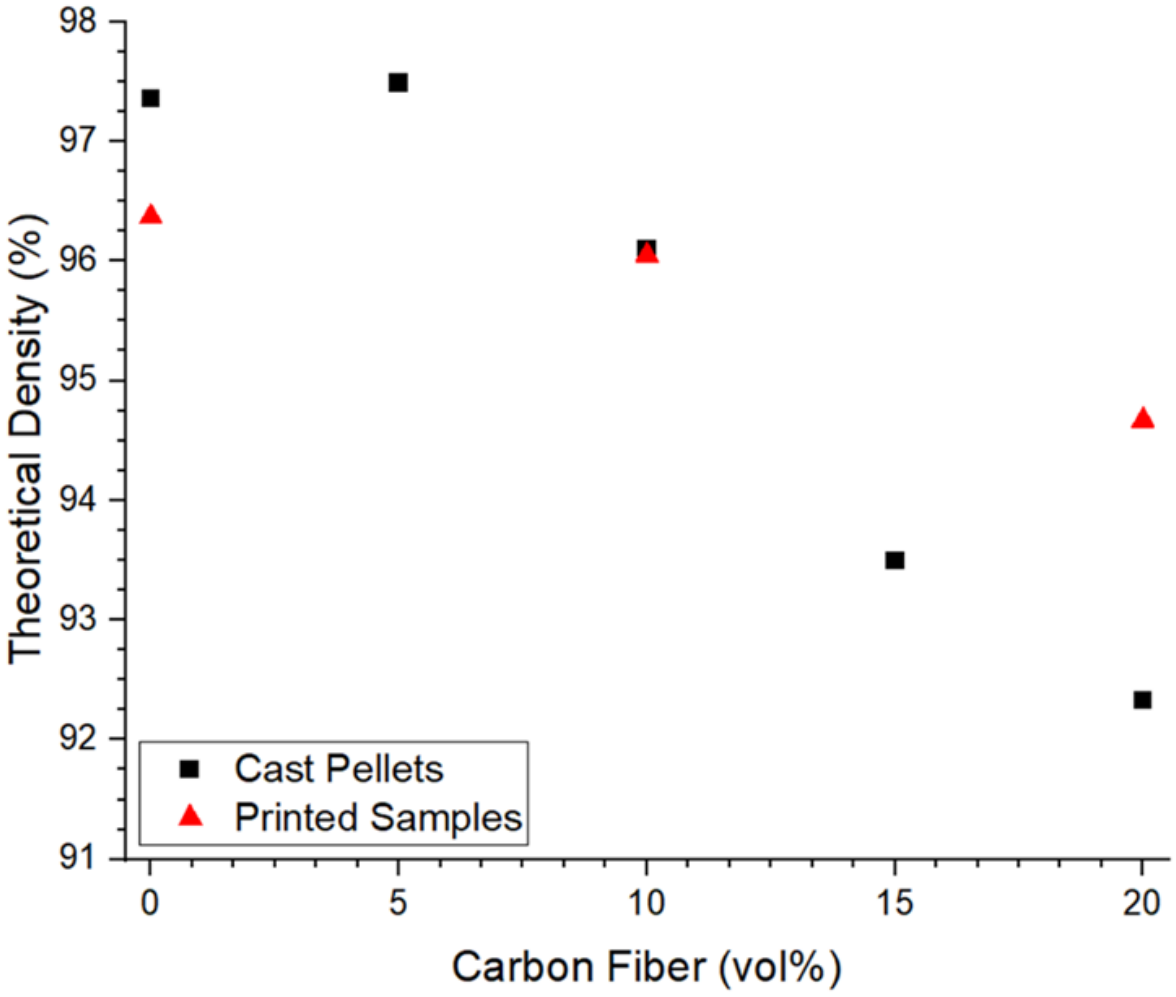

Figure 1.3. Relative densities of cast pellets and printed samples containing various amounts of carbon fiber is shown above. The theoretical density dropped below 95% between 10 vol% and 15 vol% carbon fiber addition.

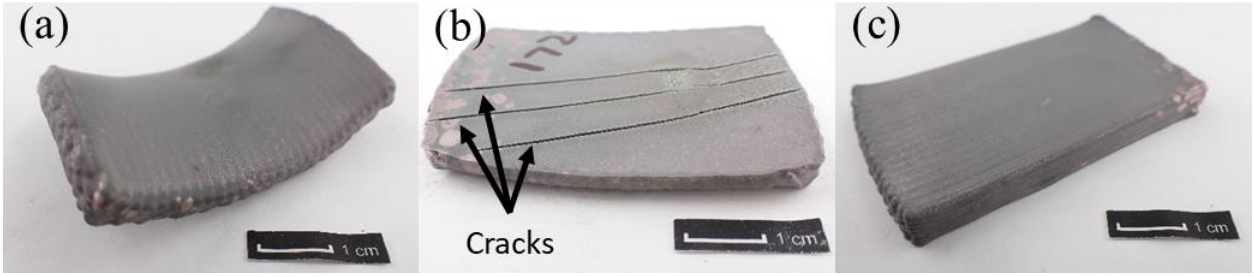

Figure 1.4. Warping and cracking was observed in C_f/SiC Rotation Prints. (a) The C_f/SiC "15º" Rotation Print warped to a saddle sintering. (b) The C_f/SiC "30º" Rotation Print with cracking on the bottom of the print and warping. (c) A C_f/SiC 0º Print, included for a reference as a print direction that did not warp or crack.

printed sample had a much higher degree of fiber alignment, especially compared to the cast pellet. Kemp et al.[19] looked at the alignment of SiC fibers in their ZrB_2-SiC matrix. They did observe fiber alignment that was due to DIW, however they did not calculate an order parameter. Fiber alignment was also noted by Franchin et al.[1] However, they did not quantify a value beyond noting the alignment.

1.3.5 Fracture Analysis

All fracture surfaces were the result of 4-point bend tests. Due to the aligned nature of the fibers, fiber pullout was observed. Figure 1.6. Shows the extent of fiber pullout for all 3 C_f/SiC print orientations. The presence of fiber pullout can indicate some degree of crack deflection. The crack deflected around the fibers as the bend bar fractured. Figure 1.6.(a) shows the full extent of fiber pullout in a 0^o C_f/SiC bend bar fracture surface. There are exposed fibers and holes form where fibers pullout out on the opposite face. Similar fiber pullout was observed during mechanical testing of other C_f/SiC samples in literature, where fibers that were aligned in the direction of the print exhibited pullout from the fracture surface.[1] Fiber pullout was not observed to the same extent for the 90^o direction as for the 0^o direction. Intergranular fracture was observed on all samples, which is typical of brittle material. Average length of fiber pullout is 14 ±4 μm as measured on a 0^o bend bar fracture surface.

1.3.6 Load Plots

Figure 1.7. shows the load plots from 2 different flexure tests. This figure compares 0^o bend bars of monolithic SiC and C_f/SiC. The monolithic SiC load plot shows typical brittle failure. The C_f/SiC plot shows a drop in force followed by reloading. This indicates crack deflection. The drop in force occurs when the crack deflects around the fibers. This behavior was only observed in C_f/SiC samples. Similar behavior was also noted by Lu et al.,[23] who created C_f/SiC using liquid silicon infiltration.

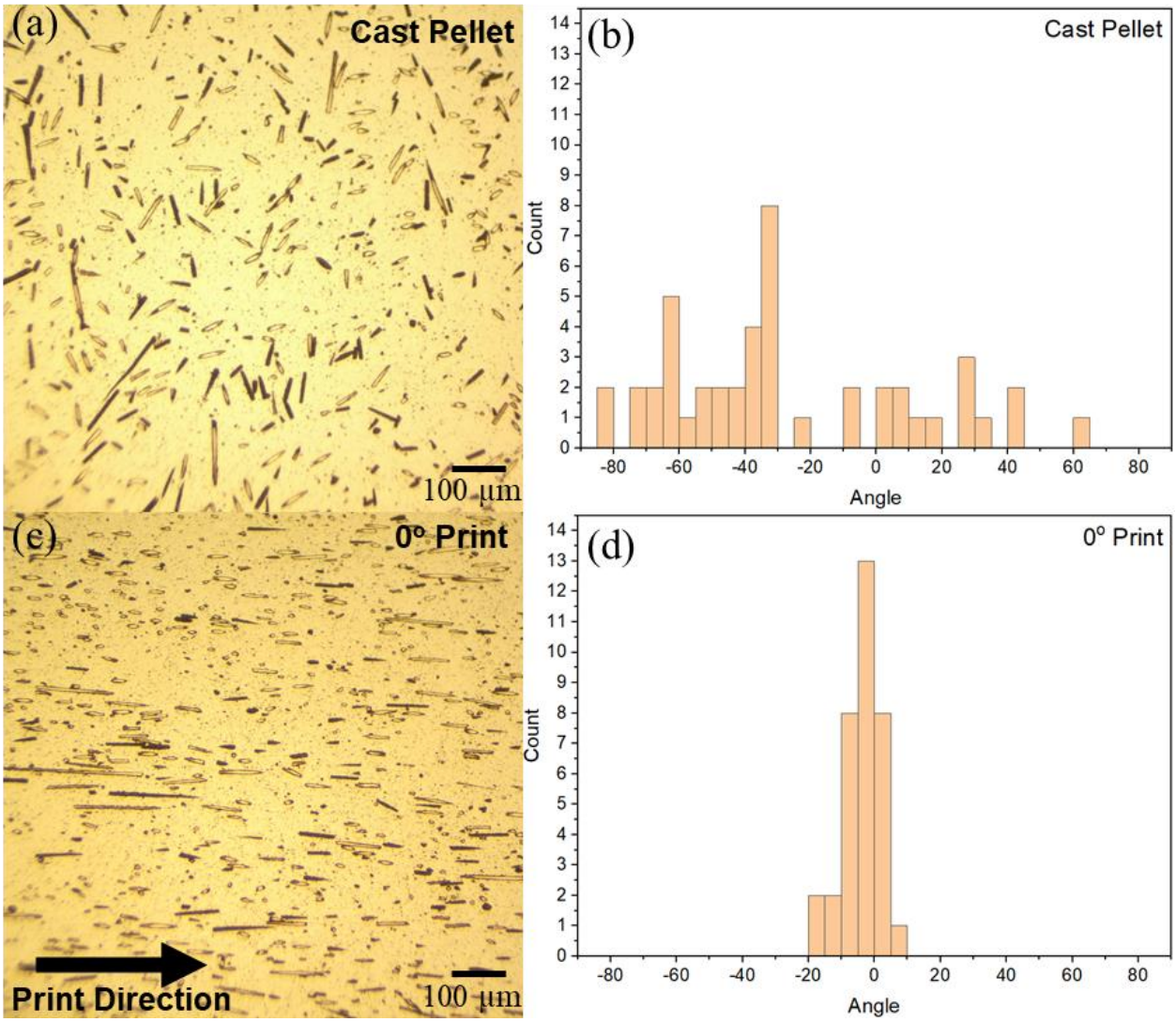

Figure 1.5. (a) An optical microscope image of cast pellet containing 10 vol% carbon fibers in a SiC matrix. The black lines are carbon fibers. (b) This distribution shows the angles of fibers from multiple spots on the pellet. (c) An optical microscope image of a C_f/SiC 0^o Print bend bar. The image was taken parallel to the print direction. (d) This distribution shows the angles of fibers from multiple spots on the bend bar.

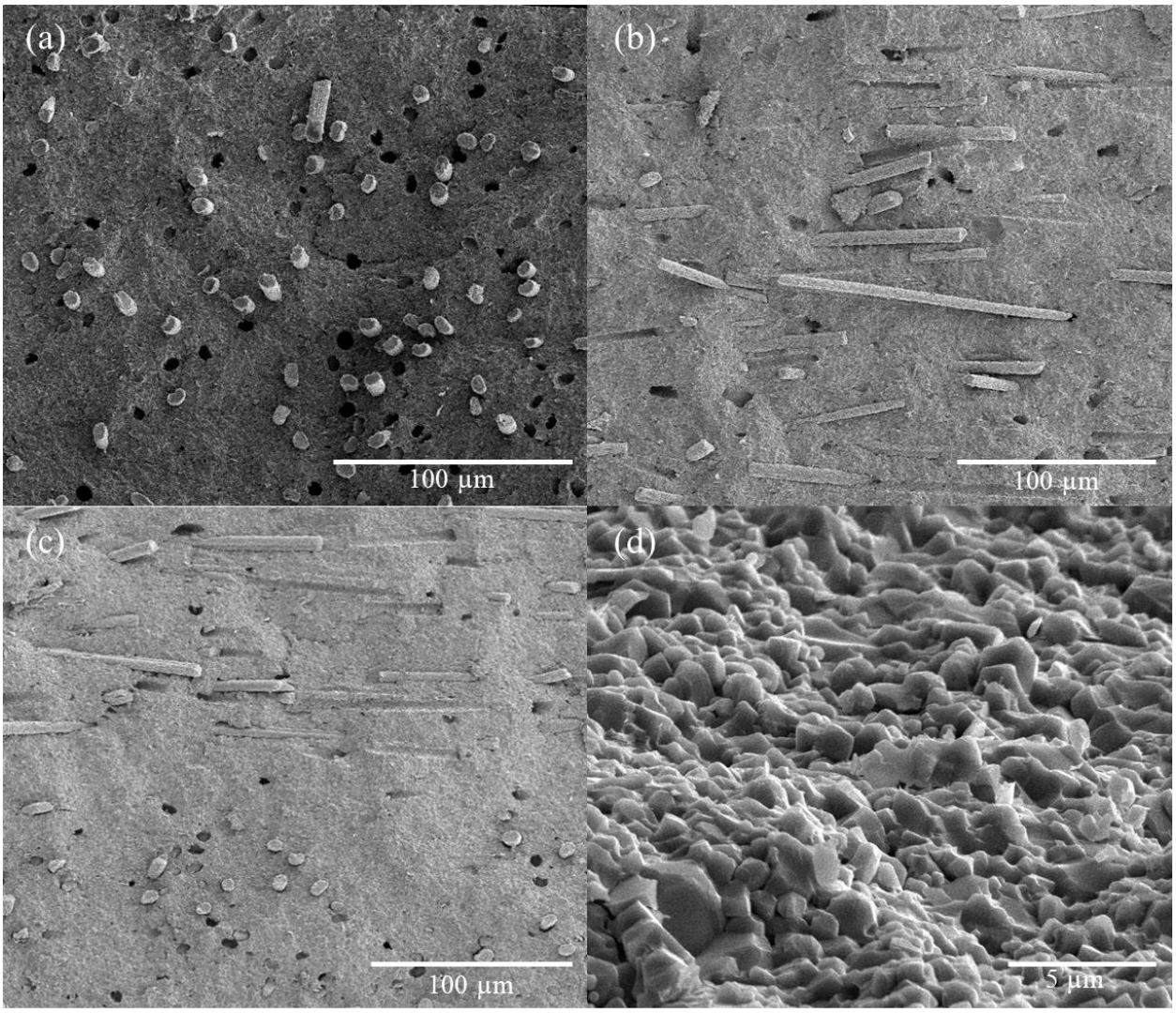

Figure 1.6. All images were taken near the tensile axis. (a) The 0º bend bar fracture surface shows fiber pullout. (b) The 90º bend bar shows a lower amount of fiber pullout in the fracture surface. (c) The interface between the 0º and 90º direction in a 0/90º sample is shown. (d) Intergranular fracture was observed on a 0º monolithic SiC bend bar fracture surface. This was observed on all facture surfaces for all samples of both monolithic SiC and C_f/SiC.

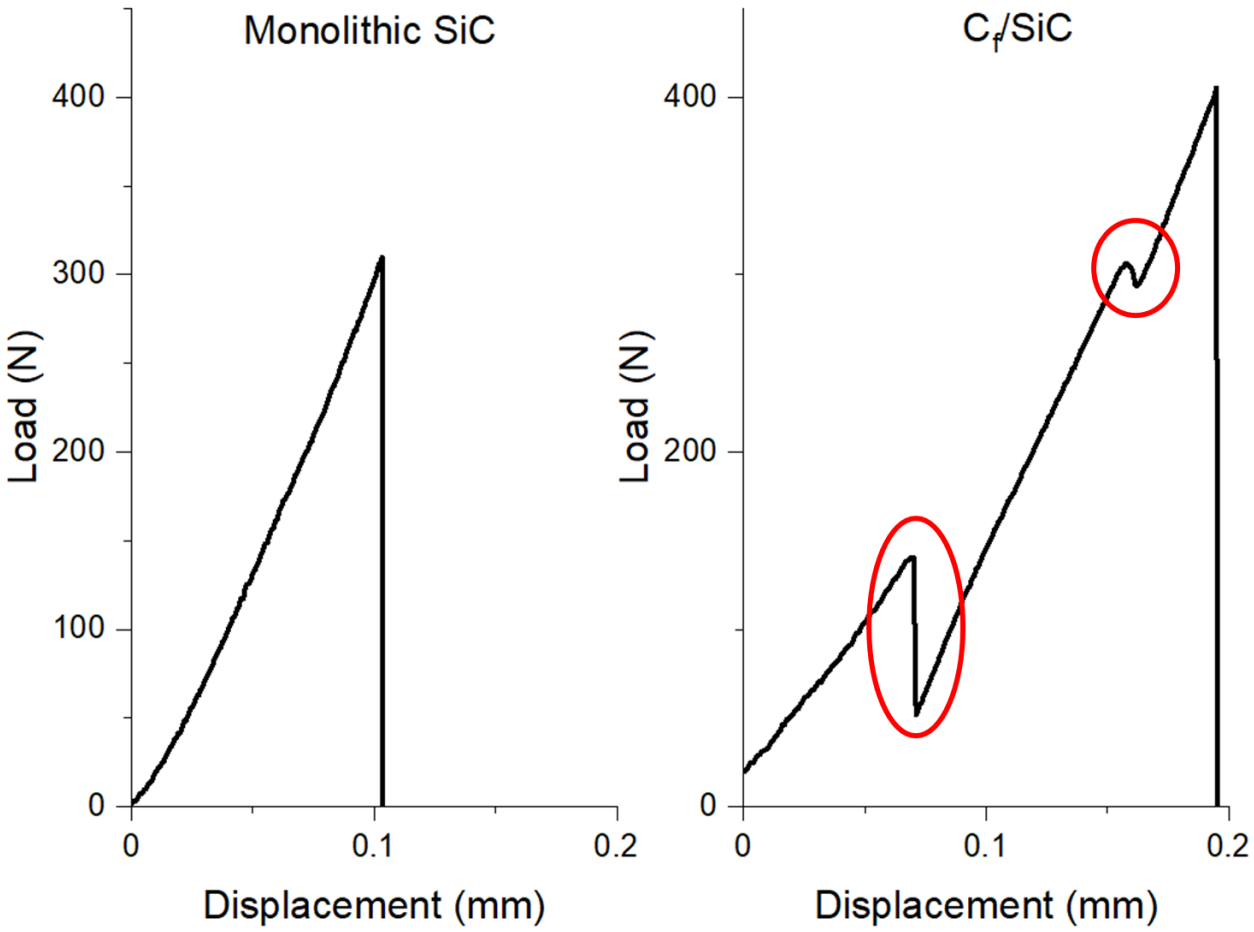

Figure 1.7. The load plot of a monolithic SiC bend bar compared to a C_f/SiC bend bar. Both bend bars are 0° Print Orientations. Circled regions highlight a drop in force followed by reloading.

Furthermore, the dropping and reloading was observed in 13/14 load plots for 0^o samples and 12/14 load plots for $0/90^o$ samples. It was only observed in 6/13 load plots for 90^o samples. This drop and reload can be associated with fiber pullout and crack deflection. This occurs more frequently in the 0^o and $0/90^o$ prints, since there is fiber alignment in the 0^o direction, which is perpendicular to the applied load, and is more readily pullout out than fibers in the 90^o direction.

1.3.7 Flexure Strength

Flexure strength was measured using 4-point bending. Stress was calculated using the peak load from testing.[28] Average strengths (σ) are shown in Table 1.1. The 0^o print orientations had the highest strength for both monolithic SiC and C_f/SiC samples. There is a modest drop in average strength from the 0^o orientation to the other orientations for monolithic SiC. There is a substantial drop in average strength between the 0^o orientation and other orientations for C_f/SiC samples. In the 0^o orientation, porosity around the fibers was offset by the large amount of fiber pullout and crack bridging observed. Since the fibers had no debond layer, there was an increase in porosity around the fibers, which caused a decrease in strength when the fibers were not aligned in the direction of the test. Fiber pullout and crack bridging was not observed to the same extent in the 90^o direction. Therefore, the lower strength associated with 90^o orientation can be attributed to the smaller amount of fiber pullout. The $0/90^o$ prints have print directions in both the 0^o and 90^o direction. Figure 1.8. shows the different print layers in a $0/90^o$ bend bar. During machining, the 0^o layers were removed to make the bar the proper thickness, leaving the 90^o direction on the surface of the bend bar. This means that 90^o direction, would be on the surface, where the tension forces are greatest during a bend test. Since there is less fiber pullout associated with the 90^o direction, the strength is similar to that of the 90^o orientation. This is the reason that both the 90^o prints and the $0/90^o$ prints have similar strengths. Both orientations have the 90^o direction on the face in tension, where failure typically begins.

The standard deviations for C_f/SiC samples were lower than for monolithic SiC samples. As discussed above, the presence of the carbon fibers induced some degree of crack bridging and crack deflection. These two mechanisms caused the bars to fail in a more consistent manner, which narrowed the standard deviation.

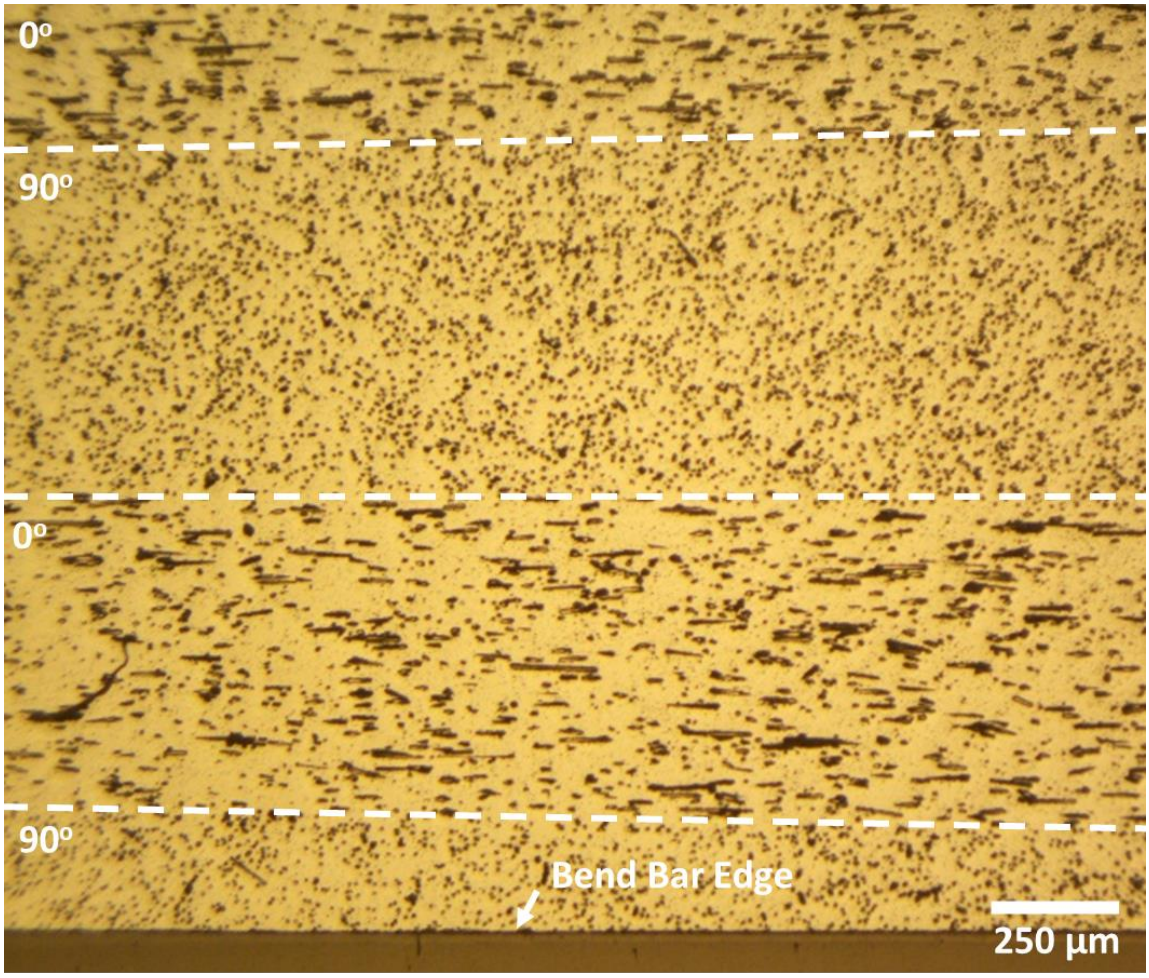

Figure 1.8. Optical microscope image of a 0/90° Print showing that the 90° direction is on the edge of the machined bend bar.

Table 1.1. Average strengths and standard deviations are shown for each print orientation, for both monolithic SiC and C_f/SiC.

	Monolithic SiC	C_f/SiC
Print Orientation	**σ_{ave} (MPa)**	**σ_{ave} (MPa)**
0°	**351 ± 54**	**343 ± 37**
90°	**322 ± 68**	**236 ± 29**
0/90°	**329 ± 52**	**240 ± 37**
"15°"	**326 ± 61**	**Not Tested**

Due to the large sample sets (13-15 bend bars), Weibull analysis was performed on the data. Figure 1.9. shows the Weibull plots for all samples. Table 1.2 shows a summary of characteristic strengths and Weibull modulus associated with each sample. The characteristic strengths for monolithic SiC samples are higher than for the C_f/SiC samples with the same print orientation. The 0° prints showed only a modest decrease in the characteristic strength of 14 MPa from monolithic SiC to C_f/SiC. The other two comparable samples, the 90° prints and the 0/90° prints showed significant decreases in the characteristic strength with the addition of carbon fiber. This decrease in strength can be attributed to the lack of a debond coating applied to the fibers. The fibers were received without any sort of coating or interface layer. No additional surface treatment was applied. Since there was no interface, there was an increase in porosity around the fibers. The lack of an interfacial layer and increased porosity combined to lower the characteristic strengths of C_f/SiC samples when compared to monolithic samples.

Table 1.2. Characteristic strengths and Weibull modulus are shown for each print orientation, for both monolithic SiC and C_f/SiC.

	Monolithic SiC		C_f/SiC	
Print Orientation	**σ_o (MPa)**	**m**	**σ_o (MPa)**	**m**
0°	**375**	**7.4**	**361**	**10.7**
90°	**351**	**4.9**	**249**	**9.2**
0/90°	**351**	**7.1**	**256**	**7.7**
"15°"	**351**	**6.2**	**Not Tested**	**Not Tested**

As shown in Table 1.2, the Weibull modulus increases for all C_f/SiC print orientations. This is also visually shown in Figure 1.9. This means that there is a smaller distribution of strengths for C_f/SiC prints due to the addition of carbon fiber.

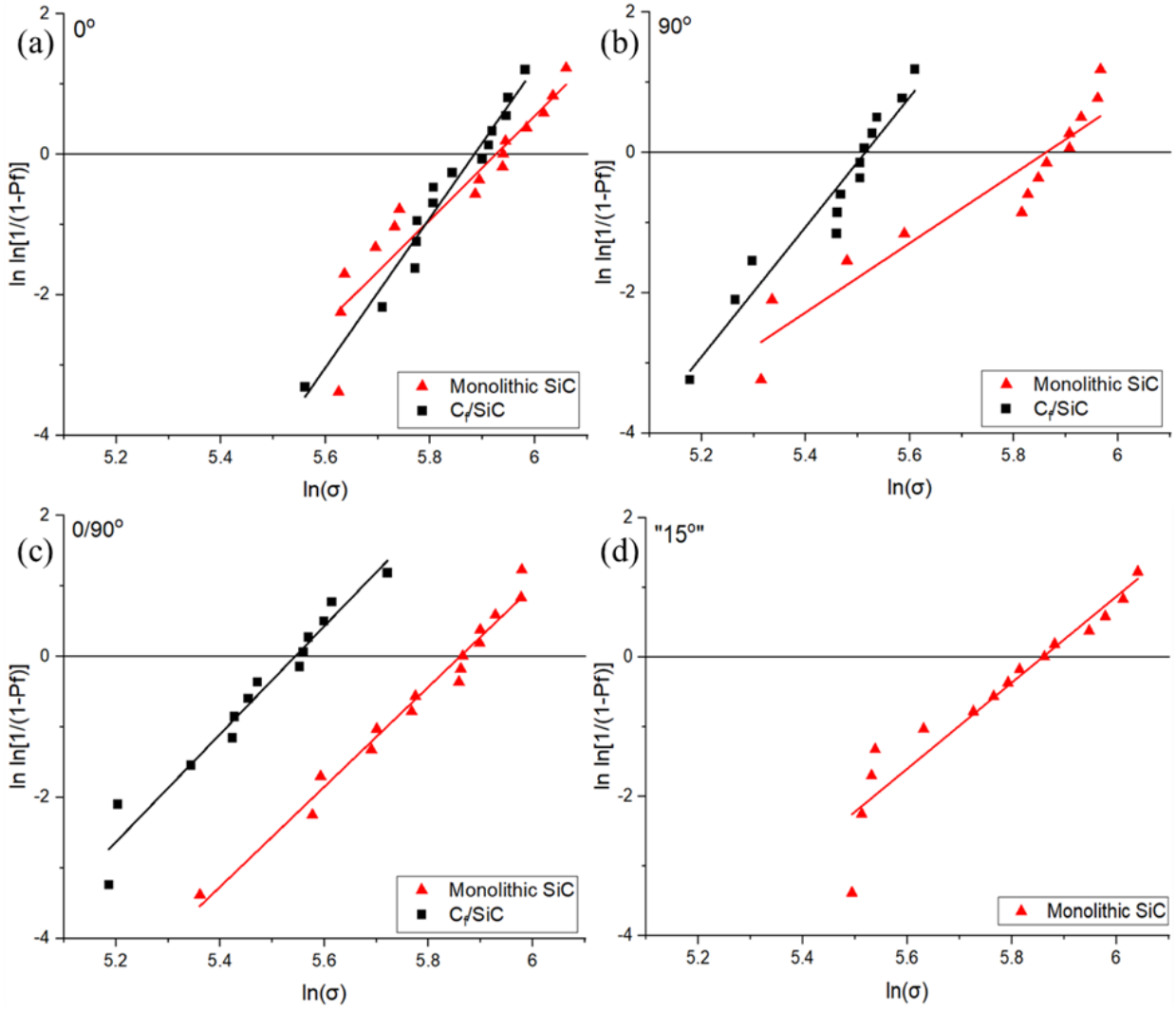

Figure 1.9. The Weibull Plots of all sets of bend bars tested. (A) 0° Print Weibull plot for both monolithic SiC and C_f/SiC. (B) A 90° Print Weibull plot for both monolithic SiC and C_f/SiC is shown. (C) A 0/90° Print Weibull plot for both monolithic SiC and C_f/SiC is shown. (D) A "15°" Print Weibull plot is shown for monolithic SiC only.

The measured strengths are comparable with reported values of other SiC. Commercially available Hexoloy SA has a reported 4-pint flexure strength of 380 MPa, a Weibull modulus of 10, and a theoretical density of >98%.[31] These values are higher than the measure values of 0º monolithic SiC tested in this study. The small increase of approximately 30 MPa and 2.6 Weibull Modulus can be attributed Hexoloy SA having a slightly higher theoretical density. Wang et al.[5] showed that by hot pressing SiC, strengths can increase up to 647 MPa. They were able to achieve densities ranging between 98.7-99.3% theoretical density. They also reported a Weibull modulus of 6.6 for their SiC, which also used Al_2O_3 and Y_2O_3 as sintering aids.[5] Both of these studies showed that densification is important for strength, and the higher the density, the higher the strengths will be.

Feilden et al.[17] created SiC parts via DIW. They were able to achieve densities of >95% theoretical density utilizing pressureless sintering with Al_2O_3 and Y_2O_3 as sintering aids. They achieved an average strength of 305 ±60 MPa for their parts. They studied print layer orientation as well. The only orientation from their study that is directly comparable is the "lengthwise" orientation. For this orientation they reported a characteristic strength of 377 MPa and a Weibull modulus of 6.1. The values reported in this study, characteristic strength of 375 MPa and Weibull modulus of 7.4 for the C_f/SiC 0º prints, are comparable.

One additional metric of interest is specific strength. Specific strength is the strength divided by the absolute density. This takes into account that the C_f/SiC has a lower absolute density than the monolithic SiC. The average strength of both the monolithic SiC and C_f/SiC 0º print orientations were divided by their respective absolute densities. The specific strength of monolithic SiC was 107 (MPa cm^3 g^{-1}) and for C_f/SiC was 109 (MPa cm^3 g^{-1}). There is a very small difference in the specific strength between monolithic SiC and C_f/SiC for the 0º direction.

1.3.8 Defects

Due to the nature of DIW, defects and porosity are inherent in the finished parts. Microporosity is created in between the print layers and individual print lines as they are laid down next to each other. Additionally, air bubbles in the suspension can cause larger pores inside of individual print layers. These defects were minimized through degassing; however, they were not entirely eliminated. Certain bend bars contained air bubbles that caused pores, and resulted in

fracture at these pores. Also, agglomerated powder or clumps of fibers can cause point defects in the SiC matrix. Samples containing these defects cannot be completely removed from the data, since these types of defects are inherent to the DIW process. However, when removed, the data can show what the mechanical properties would be like in a system without large manufacturing defects. Data was removed that came from samples that contained a defect that was visible to the naked eye. Table 1.3 shows the mechanical properties with these data points removed. As shown, the averages and standard deviations did not change in a significant way. The only significant change was to the Weibull modulus of C_f/SiC samples. They all increased with the removal of samples with a defect. This is because carbon fiber samples contained more defects due to the increased porosity around the fibers. It is also worth noting that the "15°" orientation showed a noticeable increase with the removal of samples with a defect. This is because this specific print orientation was more prone to defects than other print orientations. A total of 4 specimens were removed from this sample set, while the most removed from another sample set was 2 specimens. These additional defects result from the mismatch of the layer angles, which can lead to larger porosity at these points.

Table 1.3. Average strength, characteristic strength, and Weibull modulus for each data set shows changes in values when bend bars with visible flaws were removed.

	Monolithic SiC	**C_f/SiC**	**Monolithic SiC**		**C_f/SiC**	
Print Orientation	**σ_{ave} (MPa)**	**σ_{ave} (MPa)**	**σ_o (MPa)**	**m**	**σ_o (MPa)**	**m**
0°	**351 ± 54**	**350 ± 30**	**375**	**7.4**	**363**	**13.7**
90°	**320 ± 70**	**239 ± 27**	**350**	**4.8**	**251**	**9.7**
0/90°	**331 ± 53**	**246 ± 33**	**354**	**6.9**	**259**	**8.8**
"15°"	**351 ± 50**	**Not Tested**	**372**	**8.2**	**Not Tested**	**Not Tested**

1.4 Conclusion

A novel method for incorporating carbon fiber into a SiC matrix was demonstrated through this specific DIW process. This process was able to align milled carbon fibers in the direction of the print path, which was used to preferentially align fibers within a printed part. Parts were printed with different print layer orientations to study the effect that the print layer orientation had on a strength. Each print layer orientation was printed from both monolithic SiC and 10 vol% C_f/SiC suspensions, followed by pressureless sintering to >96% TD. The results showed that 0^o prints had a higher flexural strength than other print orientations tested. Additionally, adding milled carbon fibers in the colloidal suspension led to a decrease in flexure strength, but an increase in the Weibull modulus. There was evidence of crack deflection in parts containing carbon fiber.

There are many additional steps that could be taken to improve the properties of the printed C_f/SiC CMCs. A debond coating applied to the fibers would help transfer stress from the matrix to the fibers, which would improve the flexure strength. This could be done by using a boron nitride coating or by increasing sintering aids, which could collect around the fibers. Additionally, longer fibers or a higher fiber loading could be used to improve upon the flexure strength. Fracture toughness could be measured as another metric to analyze the C_f/SiC CMCs.

APPENDIX A. DENSIFICATION OF CAST ZRB_2-SIC VIA PRESSURELESS SINTERING

1. Introduction

Ultra-high temperature ceramics are a class of ceramics characterized by their high melting temperature. Of particular interest from this group is zirconium diboride (ZrB_2). It is extremely attractive for use due to its high melting temperature and good thermal conductivity.[12,19,32,33,34,35,36] Additionally, its relatively low density of 6.08 g/cm^3 make it an excellent candidate for aerospace and high-speed flight applications where weight is of particular concern.[12,19,32,33,34] ZrB_2 is often mixed with silicon carbide (SiC).[19,33,34] The SiC helps prevent oxidation on the surface by forming a SiO_2 layer. Additionally, the SiC can improve mechanical properties.

2. Methods

2.1. Powder Preparation

The powder used for casting was prepared by mixing 6.1 µm ZrB_2 powder (Grade B, HC Starck, Newton, MA), 600 nm β-SiC powder (US Research Nanomaterials, Houston, TX), 40-80 nm WC (US Research Nanomaterials, Houston, TX), and 2.5 µm B_4C (Hoganas, Hoganas, Sweden). The powder mixture contained 18.5 wt% (30 vol%) SiC, 8 wt% WC, 4 wt% B_4C, and 86.5 wt% ZrB_2. The WC and B_4C act as sintering aids to remove the oxide layer on the surface of the powder. The SiC acts as a reinforcement phase in the sintered ceramic. The powders were mixed in 200 proof ethanol and ball milled for 24 hours with 1 cm WC milling media at 50 rpm. After milling, the ethanol was removed by rotary evaporation followed by drying at 115 ^oC for 12 hours.

2.2. Suspension Preparation

Three different dispersants were selected for testing. The first dispersant was Darvan 821-A (Vanderbilt Chemicals, Norwalk, CT). This dispersant was combined with polyvinylpyrrolidone

(PVP, Mn 55,000, Sigma-Aldrich, US). Polyethyleneimine (PEI, Mn 10,000, Branched, Sigma-Aldrich Inc., Germany) was also used as a dispersant, both with and without the addition of PVP.

Four different suspensions were made and sintered, with various sintering parameters. The first suspension consisted of 46 vol% solids, 6.6 vol% Darvan 821-A, 1.0 vol% PVP, and balanced water.[12] The next suspension were made with 45 vol% solids, 4.5 vol% PEI, and balanced water.[36] This suspension was modified to formulate the next suspension, which contained 50 vol% solids, 4.5 vol% PEI, and balanced water. The solids loading was increased to make a more highly loaded suspension, which should increase green body density and minimizes shrinkage and cracking. The final suspension contained 50 vol% solids, 4.5 vol% PEI, 0.5 vol% PVP, and balanced water. The PVP was added as a viscosity modifier. The suspensions were mixed in a FlackTek DAC 1200-300 Speedmixer (Landrum, SC) with 2, 1 cm WC milling media. The suspensions were mixed for 2, 3-minute cycles. Each cycle had one minute at 800, 1200, and 1600 rpm. The suspensions were subsequently ball milled for 24 hours and then mixed for one additional cycle in the Speedmixer before being transferred to a syringe for casting.

2.3. Casting

Plastic molds for complex geometries were made using a FormLabs Form 3 Printer (Somerville, MA). Molds were sprayed with a silicone-based mold release agent. Pellets were cast into an RTV silicone mold. Suspensions were cast into the molds via a syringe with vibration. Cast parts were placed in a humidity oven held at 35 ^{o}C and 95% relative humidity to dry. The parts were dried in this manner to help prevent cracking.

2.4. Binder Burnout and Sintering

Binder burnout was completed in a Carbolite Gero tube furnace (Neuhausen, Germany). Samples were heated at a rate of 0.5 ^{o}C/min to 600 ^{o}C, followed by a 3-hour hold.[12] Ar was used a carrier gas.

Pressureless sintering was performed in a Carbolite Gero LHTG 200-300/301G resistively heated graphite furnace (Neuhausen, Germany). Sintering temperatures of 1950, 2050, 2100 and 2150 ^{o}C were tested with a 3-hour hold.[34,35] Additionally, 2100 ^{o}C was also tested with a 5-hour

hold. Samples were sintered using a powder bed consisting of β-SiC powder for sintering at 2150 ^{0}C only. All sintering runs started with a temperature ramp to 1450 ^{0}C at 10 ^{0}C/min with a 1 hour hold at temperature.[34] The furnace was then heated to 1650 ^{0}C at 10 ^{0}C/min with a 1 hour hold at temperature.[35] These two steps were both completed in vacuum with the intent of removing the oxide phase on the powders through the evaporation of boria (B_2O_3).[34] After the 1 hour hold at 1650 ^{0}C, the furnace was filled with Ar and was heated to the selected sintering temperature at 20 ^{0}C/min. After the specified hold time, either 3 hours or 5 hours, the samples were cooled to room temperature, with the atmosphere remaining Ar through the hold and cooling steps. All densities were calculated using Archimedes' method. The theoretical density of a sintered ZrB_2-SiC part is 5.19 g/cm^3 with 30 vol% SiC.

3. Discussion

3.1. Density

Table A.1. shows all relative densities based on the final sintering temperature, hold time, and presence of powder bed. As shown, increased sintering temperature increased relative density. Additionally, increasing the hold time also increased the density. The presence of a powder bed only slightly increased the density; however, it did work to minimize surface cracking. The surface cracking was partly influenced by uneven heating of the part, where the surface heated and shrunk before the center was heated to the same temperature. The powder bed offered a more even heating rate to the pellet and minimized cracking from sintering. The powder bed cannot consist of the original powder, as it will sinter to the parts and prevent removal of sintered pellets. The optimum sintering parameters were heating to 2150 ^{o}C for 3 hours with a SiC powder bed.

Table A.1. The percent theoretical densities of the cast pellets organized by the suspension formulation and sintering temperature is shown.

	3 Hour Hold				Powder Bed	5 Hour Hold
Formulation	1950 ^{o}C	2050 ^{o}C	2100 ^{o}C	2150 ^{o}C	2150 ^{o}C	2100 ^{o}C
46 vol% ZrB2/Darvan, PVP	62.3%	78.6%	88.6%			
45 vol% ZrB2/PEI		81.7%	88.9%			
50 vol% ZrB2/PEI	64.4%	82.7%	89.4%	95.6%		92.5%
50 vol% ZrB2/PEI, PVP				94.6%	95.6%	92.8%

3.2. Shrinkage and Cracking

The parts experienced an average of 15.43% shrinkage during sintering, with a range of 15.3% to 15.9%. Additionally, parts experienced a small degree of surface cracking during sintering. This is caused by residual stresses that occur during drying as the part experiences uneven drying. To mitigate these problems, samples were dried in a humidity oven

After drying in a humidity oven, the samples still exhibited cracking. Figure A.1. shows an example of cracking observed. The cracking was thought to be a result of the cast parts being too thick. However, cracking was still observed, even in parts as thin as 3 mm. Green body cracking in a thin part can be caused by issues with the mold or with the suspension. Since special care was taken to prevent adhesion to the mold, the likely cause of the cracking is due to the suspensions. Since a relatively highly loaded suspension was used, cracking could result from poor dispersion of the powders. This would lead to an unstable green body that is prone to cracking. If there are cracks in the green body, then there will be cracks in the sintered part.

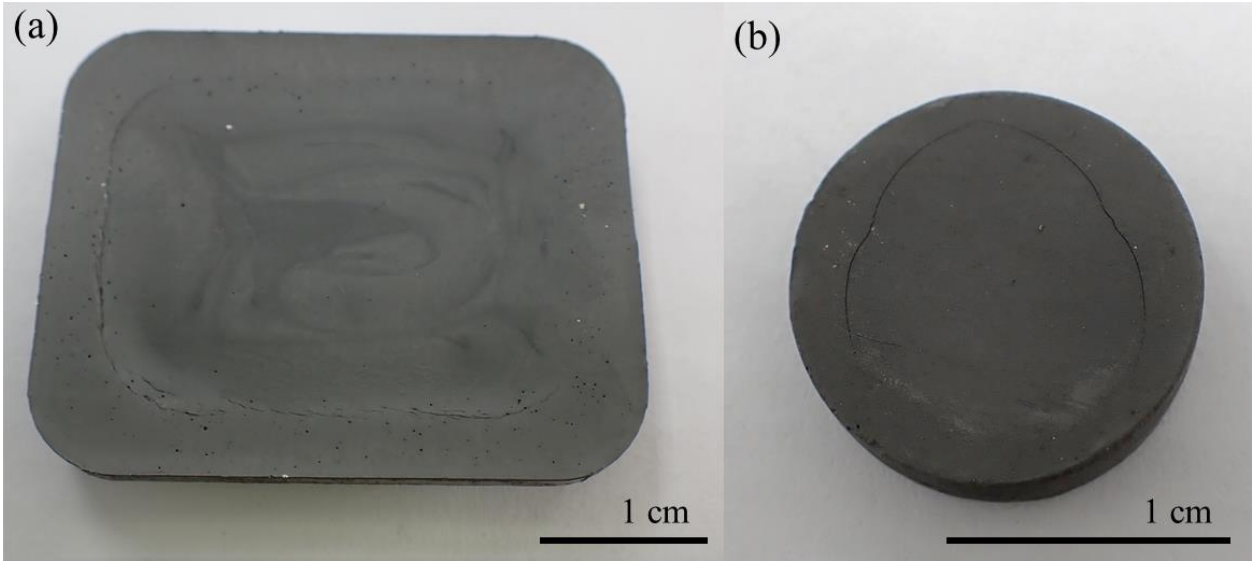

Figure A.1. (a) A green body displaying cracking. (b) A brown body displaying cracking.

4. Conclusion

ZrB_2-SiC UHTC can be sintered to a high density using pressureless sintering. An aqueous suspension cast into pellets was shown to reach high density (>95% TD) using B_4C and WC as

sintering aids. During sintering, the holds at 1450 ^{0}C and 1650 ^{0}C under vacuum allowed for the removal of B_2O_3 and other oxide phases. This facilitated the removal of the oxide coating on the powders and ultimately, improved densification. Additionally, a powder bed helped increase the density by creating a more even heating profile. Consistent shrinkage was observed. Cracking was also a constant issue.

Future work should focus on trying different suspensions. The main focus should be around suspensions using Darvan 821-A as the dispersant. Once a suspension is created that does not crack upon drying, the sintering method developed in this work can be used to create highly dense parts.

REFERENCES

[1] G. Franchin, L. Wahl, P. Colombo, Direct ink writing of ceramic matrix composite structures, J. Am. Ceram. Soc., 100(10) (2017) 4397–4401, https://doi.org/10.1111/jace.15045.

[2]K. Cai, B. Román-Manso, J. E. Smay, J. Zhou, M. I. Osendi, M. Belmonte, P. Miranzo, Geometrically complex silicon carbide structures fabricated by robocasting, J. Am. Ceram. Soc., 95(8) (2012) 2660–2666, https://doi.org/10.1111/j.1551-2916.2012.05276.

[3] T. D. Gulden, Mechanical Properties of B-SiC, J. Am. Ceram. Soc., 52(11) (1969) 585–590.

[4] Y. Katoh, L. L. Snead, C. H. Henager, T. Nozawa, T. Hinoki, A. Iveković, S. Novak, S. M. Gonzalez De Vicente, Current status and recent research achievements in SiC/SiC composites. J. Nucl. Mater., 455(1–3) (2014) 387–397, https://doi.org/10.1016/j.jnucmat.2014.06.003.

[5] X. H. Wang, Y. Hirata, Influence of polyacrylic acid on rheology of SiC suspension and mechanical properties of densified SiC, Ceram. Int., 31(5) (2005) 677–681, https://doi.org/10.1016/j.ceramint.2004.08.006.

[6] L. F. Francis, C. C. Roberts, Dispersion and Solution Processes, Mater. Process., (2016) 415–512, https://doi.org/10.1016/b978-0-12-385132-1.00006-9.

[7] J. A. Lewis, Colloidal Processing of Ceramic, J. Am. Ceram. Soc., 83(10) (2000) 2341–2359.

[8] V. L. Wiesner, J. P. Youngblood, R. W. Trice, Room-temperature injection molding of aqueous alumina-polyvinylpyrrolidone suspensions, J. Euro. Ceram. Soc., 34(2) (2014) 453–463, https://doi.org/10.1016/j.jeurceramsoc.2013.08.017.

[9] L. M. Rueschhoff, R. W. Trice, J. P. Youngblood, Near-net shaping of silicon nitride via aqueous room-temperature injection molding and pressureless sintering, Ceram. Int., 43(14) (2017) 10791–10798, https://doi.org/10.1016/j.ceramint.2017.05.097.

[10] L. M. Rueschhoff, J. P. Youngblood, R. W. Trice, R. Bordia, Stabilizing Highly Loaded Silicon Nitride Aqueous Suspensions Using Comb Polymer Concrete Superplasticizers J. Am. Ceram. Soc., 99(12) (2016) 3857–3865, https://doi.org/10.1111/jace.14432.

[11] A. Diaz-Cano, R. W. Trice, J. P. Youngblood, Stabilization of highly-loaded boron carbide aqueous suspensions, Ceram. Int., 43(12) (2017) 8572–8578, https://doi.org/10.1016/j.ceramint.2017.03.111.

[12] V. L. Wiesner, L. M. Rueschhoff, A. I. Diaz-Cano, R. W. Trice, J. P. Youngblood, Producing dense zirconium diboride components by room-temperature injection molding of aqueous ceramic suspensions, Ceram. Int., 42(2) (2016) 2750–2760, https://doi.org/10.1016/j.ceramint.2015.11.005.

[13] M. Xia, J. Sanjayan, Method of formulating geopolymer for 3D printing for construction applications, Mater. and Des., 110 (2016) 382–390. https://doi.org/10.1016/j.matdes.2016.07.136.

[14] A. Zocca, P. Lima, S. Diener, N. Katsikis, J. Günster, Additive manufacturing of SiSiC by layerwise slurry deposition and binder jetting (LSD-print), J. Euro. Ceram. Soc., 39(13) (2019) 3527–3533, https://doi.org/10.1016/j.jeurceramsoc.2019.05.009.

[15] W. J. Costakis, L.M. Rueschhoff, A. I. Diaz-Cano, J. P. Youngblood, R. W. Trice, Additive manufacturing of boron carbide via continuous filament direct ink writing of aqueous ceramic suspensions, J. Euro. Ceram. Soc., 36(14) (2016) 3249–3256, https://doi.org/10.1016/j.jeurceramsoc.2016.06.002.

[16] J. S. Pelz, N. Ku, W. T. Shoulders, M. A. Meyers, L. R. Vargas-Gonzalez, Multi-material additive manufacturing of functionally graded carbide ceramics via active, in-line mixing, Addit. Manuf., 37 (2021) 101647-101658, https://doi.org/10.1016/j.addma.2020.101647.

[17] E. Feilden, E. G. T. Blanca, F. Giuliani, E. Saiz, L. Vandeperre, Robocasting of structural ceramic parts with hydrogel inks, J. Euro. Ceram. Soc., 36(10) (2016) 2525–2533, https://doi.org/10.1016/j.jeurceramsoc.2016.03.001.

[18] L. Rueschhoff, W. Costakis, M. Michie, J. Youngblood, R. Trice, Additive Manufacturing of Dense Ceramic Parts via Direct Ink Writing of Aqueous Alumina Suspensions, Int. J. Appl. Ceram. Technol., 13(5) (2016) 821–830, https://doi.org/10.1111/ijac.12557.

[19] J. W. Kemp, A. A. Diaz, E. C. Malek, B. P. Croom, Z. D. Apostolov, S. R. Kalidindi, B. G. Compton, L. M. Rueschhoff, Direct ink writing of ZrB2-SiC chopped fiber ceramic composites, Addit. Manuf., 44 (2021) 102049-102058, https://doi.org/10.1016/j.addma.2021.102049.

[20] S. H. Bong, B. Nematollahi, A. Nazari, M. Xia, J. G. Sanjayan, Fresh and hardened properties of 3D printable geopolymer cured in ambient temperature, RILEM Bookseries, 19 (2019) 3–11, https://doi.org/10.1007/978-3-319-99519-9_1.

[21] M. Moini, J. Olek, J. P. Youngblood, B. Magee, P. D. Zavattieri, Additive Manufacturing and Performance of Architectured Cement-Based Materials, Adv. Mater., 30(43) (2018) 1802123-1802134, https://doi.org/10.1002/adma.201802123.

[22] S. Ketel, G. Falzone, B. Wang, N. Washburn, G. Sant, A printability index for linking slurry rheology to the geometrical attributes of 3D-printed components, Cement and Concrete Composites, 101 (2019) 32–43, https://doi.org/10.1016/j.cemconcomp.2018.03.022.

[23] Z. Lu, Y. Xia, K. Miao, S. Li, L. Zhu, H. Nan, J. Cao, D. Li, Microstructure control of highly oriented short carbon fibres in SiC matrix composites fabricated by direct ink writing, Ceram. Int., 45(14) (2019) 17262–17267, https://doi.org/10.1016/j.ceramint.2019.05.283.

[24] A. Zocca, G. Franchin, H. Elsayed, E. Gioffredi, E. Bernardo, P. Colombo, A. Bandyopadhyay, Direct Ink Writing of a Preceramic Polymer and Fillers to Produce Hardystonite (Ca2ZnSi2O7) Bioceramic Scaffolds, J. Am. Ceram. Soc., 99(6) (2016) 1960–1967, https://doi.org/10.1111/jace.14213.

[25] H. Xiong, H. Chen, L. Zhao, Y. Huang, K. Zhou, D. Zhang, SiC w /SiC p reinforced 3D-SiC ceramics using direct ink writing of polycarbosilane-based solution: Microstructure, composition and mechanical properties, J. Euro. Ceram. Soc., 39(8) (2019) 2648–2657, https://doi.org/10.1016/j.jeurceramsoc.2019.02.045.

[26] V. Wiesner, M. Acosta, L. Rueschhoff, J. Youngblood, R. Trice, Horizontal Dip-Spin Casting of aqueous alumina-polyvinylpyrrolidone suspensions with chopped fiber, Int. J. Appl. Ceram. Technol., 14(6) (2017) 1077–1087, https://doi.org/10.1111/ijac.12714.

[27] B. P. Croom, A. Abbott, J. W. Kemp, L. Rueschhoff, L. Smieska, A. Woll, S. Stoupin, H. Koerner, Mechanics of nozzle clogging during direct ink writing of fiber-reinforced composites, Addit. Manuf., 37 (2021), 101701-101712, https://doi.org/10.1016/j.addma.2020.101701.

[28] Standard Test Method for Flexural Strength of Advanced Ceramics at Ambient Temperature, (2018), https://doi.org/10.1520/C1161-18.

[29] J. A. Diaz, X. Wu, A. Martini, J. P. Youngblood, R. J. Moon, Thermal expansion of self-organized and shear-oriented cellulose nanocrystal films, Biomacromolecules, 14(8) (2013) 2900–2908, https://doi.org/10.1021/bm400794e.

[30] R. A. Chowdhury, S. X. Peng, J. Youngblood, Improved order parameter (alignment) determination in cellulose nanocrystal (CNC) films by a simple optical birefringence method, Cellulose, 24(5) (2017) 1957–1970, https://doi.org/10.1007/s10570-017-1250-9.

[31] Hexoloy® SA Silicon Carbide Technical Data, (2012).

[32] W. G. Fahrenholtz, G. E. Hilmas, S. C. Zhang, S. Zhu, Pressureless sintering of zirconium diboride: Particle size and additive effects, J. Am. Ceram. Soc., 91(5) (2008) 1398–1404, https://doi.org/10.1111/j.1551-2916.2007.02169.

[33] H. Zhang, Y. Yan, Z. Huang, X. Liu, D. Jiang, Pressureless sintering of ZrB2-SiC ceramics: the effect of B4C content, Scr. Mater., 60(7) (2009) 559–562, https://doi.org/10.1016/j.scriptamat.2008.12.003.

[34] S. C. Zhang, G. E. Hilmas, W. G. Fahrenholtz, Pressureless sintering of ZrB2-SiC ceramics, J. Am. Ceram. Soc., 91(1) (2008) 26–32, https://doi.org/10.1111/j.1551-2916.2007.02006.

[35] A. L. Chamberlain, W. G. Fahrenholtz, G. E. Hilmas, Pressureless sintering of zirconium diboride, J. Am. Ceram. Soc., 89(2) (2006) 450–456, https://doi.org/10.1111/j.1551-2916.2005.00739.

[36] S. H. Lee, Y. Sakka, Y. Kagawa, Dispersion behavior of ZrB2 powder in aqueous solution, J. Am. Ceram. Soc., 90(11) (2007) 3455–3459, https://doi.org/10.1111/j.1551-2916.2007.01949.